JACS
JOURNAL OF THE AMERICAN CHEMICAL SOCIETY
Article
pubs.acs.org/JACS

Supramolecular Coordination Polymer Formed from Artificial Light-Harvesting Dendrimer

Hosoowi Lee,[†] Young-Hwan Jeong,[†] Joo-Ho Kim,[†] Inhye Kim,[‡] Eunji Lee,*[,‡] and Woo-Dong Jang*[,†]

[†]Department of Chemistry, Yonsei University, 50 Yonsei-ro, Seodaemun-gu, Seoul 120-749, Korea

[‡]Graduate School of Analytical Science and Technology, Chungnam National University, 99 Daehak-ro, Yuseong-gu, Daejeon 305-764, Korea

Supporting Information

ABSTRACT: We report the formation of supramolecular coordination polymers formed from multiporphyrin dendrimers ($\mathbf{P_{Zn}P_M}$; **M** = **FB** or **Cu**), composed of the focal freebase porphyrin ($\mathbf{P_{FB}}$) or cupper porphyrin ($\mathbf{P_{Cu}}$) with eight zinc porphyrin ($\mathbf{P_{Zn}}$) wings, and multipyridyl porphyrins ($\mathbf{PyP_M}$; **M** = **FB** or **Cu**), $\mathbf{P_{FB}}$ or $\mathbf{P_{Cu}}$ with eight pyridyl groups, through multiple axial coordination interactions of pyridyl groups to $\mathbf{P_{Zn}}$s. UV−vis absorption spectra were recorded upon titration of $\mathbf{PyP_{FB}}$ to $\mathbf{P_{Zn}P_{FB}}$. Differential spectra, obtained by subtracting the absorption of $\mathbf{P_{Zn}P_{FB}}$ without guest addition as well as the absorption of $\mathbf{PyP_{FB}}$, exhibited clear isosbestic points with saturation binding at 1 equiv addition of $\mathbf{PyP_{FB}}$ to $\mathbf{P_{Zn}P_{FB}}$. Job's plot analysis also indicated 1:1 stoichiometry for the saturation binding. The apparent association constant between $\mathbf{P_{Zn}P_{FB}}$ and $\mathbf{PyP_{FB}}$ ($2.91 \times 10^6\ M^{-1}$), estimated by isothermal titration calorimetry, was high enough for fibrous assemblies to form at micromolar concentrations. The formation of a fibrous assembly from $\mathbf{P_{Zn}P_{FB}}$ and $\mathbf{PyP_{FB}}$ was visualized by atomic force microscopy and transmission electron microscopy (TEM). When a 1:1 mixture solution of $\mathbf{P_{Zn}P_{FB}}$ and $\mathbf{PyP_{FB}}$ (20 μM) in toluene was cast onto mica, fibrous assemblies with regular height (ca. 2 nm) were observed. TEM images obtained from 1:1 mixture solution of $\mathbf{P_{Zn}P_{FB}}$ and $\mathbf{PyP_{FB}}$ (0.1 wt %) in toluene clearly showed the formation of nanofibers with a regular diameter of ca. 6 nm. Fluorescence emission measurement of $\mathbf{P_{Zn}P_M}$ indicated efficient intramolecular energy transfer from $\mathbf{P_{Zn}}$ to the focal $\mathbf{P_{FB}}$ or $\mathbf{P_{Cu}}$. By the formation of supramolecular coordination polymers, the intramolecular energy transfer changed to intermolecular energy transfer from $\mathbf{P_{Zn}P_M}$ to $\mathbf{PyP_M}$. When the nonfluorescent $\mathbf{PyP_{Cu}}$ was titrated to fluorescent $\mathbf{P_{Zn}P_{FB}}$, fluorescence emission from the focal $\mathbf{P_{FB}}$ was gradually decreased. By the titration of fluorescent $\mathbf{PyP_{FB}}$ to nonfluorescent $\mathbf{P_{Zn}P_{Cu}}$, fluorescence emission from $\mathbf{P_{FB}}$ in $\mathbf{PyP_{FB}}$ was gradually increased due to the efficient energy transfer from $\mathbf{P_{Zn}}$ wings in $\mathbf{P_{Zn}P_{Cu}}$ to $\mathbf{PyP_{FB}}$.

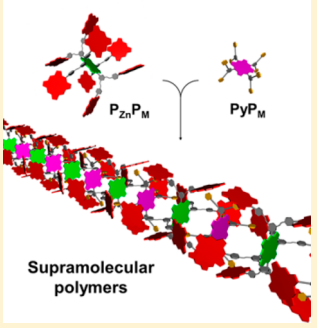

INTRODUCTION

The formation of supramolecular polymers is considered as an emerging technology in the fields of structural, electronic, biomedical, and biomimetic functional materials science.[1−3] Various molecular interactions, including multiple hydrogen bonds, host−guest inclusions, $\pi-\pi$ interactions, metal-coordination interaction, and so on, have been applied to build supramolecular polymers.[4−8] Among various interactions, metal-coordination interaction is particularly interesting because metal-coordination bonds form highly directional and controllable manner.[9−11] Metalloporphyrins often form well-ordered supramolecular architectures through the axial coordination interaction between the central metal ion and pyridyl ligands.[12] The biological importance and relevance of porphyrins have made multiporphyrin arrays of great interest from a biomimetic standpoint.[13−19] Especially, natural light-harvesting antenna complexes (LHCs) in plants and bacteria are composed of a great number of self-assembled porphyrin-based chromophore units that efficiently absorb visible photons to initiate the conversion of solar energy to vital energy sources.[20,21] Large number of porphyrin-based chromophores in LHCs create a sequence of photochemical processes, i.e., light absorption, energy migration and energy transfer to reaction center, charge separation, and electron transfer.[20] To mimic LHCs, synthetic chemists have synthesized multi-porphyrin-incorporated molecules for efficient light absorption, directed energy transfer, charge separation, and photocatalytic reactions.[15,19,22−29] In addition to covalent approaches, scientists have also attempted to create porphyrin-based supramolecular assemblies that mimic LHCs.[12,19,27,30−33] For example, Herz et al. reported porphyrin nanorings as the biomimetic example of light-harvesting antenna.[32] Hupp et al. reported porphyrin-based metal−organic frameworks to achieve efficient light-harvesting and ultrafast energy migration.[33] We recently reported artificial light-harvesting dendrimers with multiple zinc porphyrin ($\mathbf{P_{Zn}}$) wings connected to the focal freebase porphyrin ($\mathbf{P_{FB}}$).[30] These porphyrin dendrimers exhibited very efficient energy transfer from the $\mathbf{P_{Zn}}$ wings to the focal $\mathbf{P_{FB}}$. Moreover, formation of host−guest complexes between the porphyrin dendrimers and pyridyl-bearing porphyrins enabled photophysical switching from energy transfer to electron transfer. Such supramolecular assembly-based photophysical switching would provide critical

Received: August 1, 2015
Published: September 8, 2015

ACS Publications © 2015 American Chemical Society

DOI: 10.1021/jacs.5b08092
J. Am. Chem. Soc. 2015, 137, 12394−12399

benefits for the design of effective porphyrin-based functional nanomaterials.[34,35] In this context, we demonstrate the formation of supramolecular coordination polymers formed from artificial light-harvesting porphyrin dendrimers ($\mathbf{P_{Zn}P_M}$; **M** = **FB** or **Cu**; Scheme 1) and pyridyl-bearing porphyrins ($\mathbf{PyP_M}$; **M** = **FB** or **Cu**; Schemes 1 and 2).

Scheme 1. Chemical Structures of Multiporphyrin Dendrimers ($P_{Zn}P_M$) and Multipyridyl Porphyrins (PyP_M) and Schematic Illustration of Supramolecular Polymers

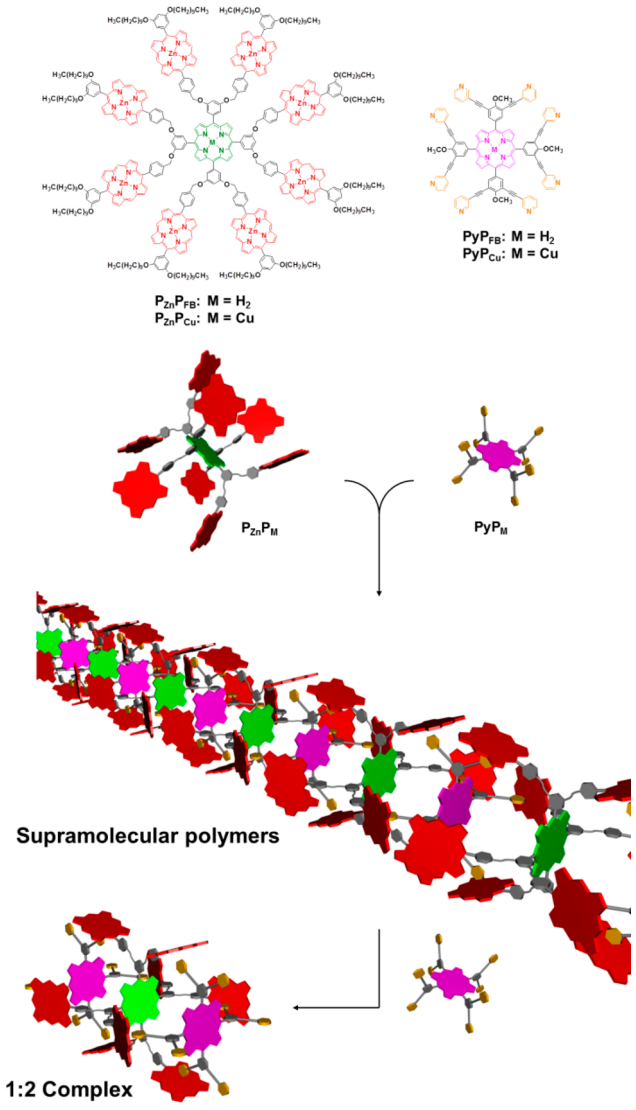

EXPERIMETAL SECTION

Materials and Measurements. All commercially available reagents were reagent grade and used without further purification. CH_2Cl_2, *n*-hexane, and tetrahydrofuran (THF) were freshly distilled before each use. UV–vis absorption spectra were recorded on a JASCO V-660 spectrometer. Fluorescence spectra were measured by a JASCO FP-6300 spectrophotometer, and spectral sensitivity was corrected by comparison with well-known chromophores such as rhodamine and coumarin dyes. All spectral measurements were carried out using a quartz cuvette with a path length of 1 cm at ambient temperature. ^{1}H NMR spectra were recorded at 25 °C on a Bruker DPX 400 and a Bruker Avance 600 spectrometer, and ^{13}C NMR spectra were recorded at 25 °C on a Bruker DPX 400 spectrometer. 2D-DOSY NMR spectra were recorded at 25 °C on a Bruker Avance 600 spectrometer. MALDI-TOF-MS was performed on a Bruker Daltonics LRF20 with dithranol (1,8,9-trihydroxyanthracene) as the matrix. Gel permeation chromatography (GPC) was performed on JAI model LC9201 equipped with JAIGEL-2H and JAIGEL-3H columns using $CHCl_3$ as the eluent. Isothermal titration calorimetry (ITC) was performed on a Microcal VP-ITC. Atomic force microscopy (AFM) images were obtained using a VEECO MULTIMODE instrument. Transmission electron microscopy (TEM) images were taken using a JEOL JEM_3011 HR and a JEOL JEM-1400.

Scheme 2. Synthesis of PyP_M[a]

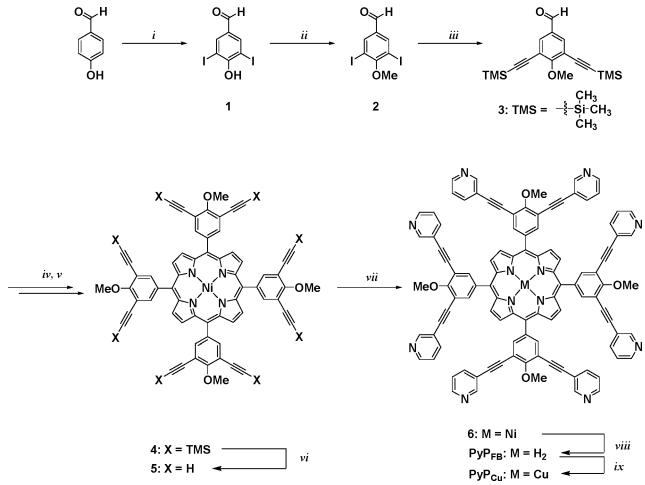

[a]Reagents and conditions; (i) $NaIO_4$, NaCl, KI, AcOH/H_2O, 2 day, 25 °C; (ii) K_2CO_3, CH_3I, DMF, 13 h, 25 °C; (iii) $Pd(PPh_3)_2Cl_2$, CuI, trimethylsilylacetylene, diisopropylamine, 48 h, 25 °C, (iv) pyrrole, propionic acid, reflux, 4 h; (v) nickel(II) acetylacetonate, toluene, reflux, 12 h; (vi) tetrabutylammonium fluoride, THF, 24 h, 25 °C; (vii) $Pd(PPh_3)_2Cl_2$, 3-iodopyridine, diisopropylamine/THF (2:1), 2 day, 70 °C; (viii) H_2SO_4, CH_2Cl_2/MeOH/THF (5:1:1), 30 m, 25 °C; (ix) $Cu(OAc)_2{\cdot}H_2O$, MeOH/CH_2Cl_2, 3 h, 25 °C.

UV–vis Titration. UV–vis absorption spectra of $\mathbf{P_{Zn}P_{FB}}$ and $\mathbf{PyP_{FB}}$ were recorded upon titration of $\mathbf{PyP_{FB}}$. Then, differential spectra were obtained by subtracting the absorption of $\mathbf{P_{Zn}P_{FB}}$ without $\mathbf{PyP_{FB}}$ addition as well as the absorption of $\mathbf{PyP_{FB}}$. Because a fixed volume of $\mathbf{PyP_{FB}}$ solution was continuously added, the total absorption of $\mathbf{PyP_{FB}}$ could be numerically calculated from the standard solution. The total volume of mixture solution increased gradually, but the concentration of $\mathbf{P_{Zn}P_{FB}}$ gradually decreased upon continuous addition of $\mathbf{PyP_{FB}}$ solution. Therefore, the final spectra were divided into dilution factors for each titration step to display the UV–vis titration spectra and binding isotherms.

Isothermal Titration Calorimetry (ITC). ITC experiments were conducted on a Microcal VP-ITC at 25 °C. For ITC measurements, toluene solutions of $\mathbf{P_{Zn}P_{FB}}$ (4.2×10^{-5} M) and $\mathbf{PyP_{FB}}$ (5.4×10^{-4} M) were prepared. Both solutions were degassed at 25 °C before measurements. Six μL of $\mathbf{PyP_{FB}}$ solution in the injection syringe was successively injected to $\mathbf{P_{Zn}P_{FB}}$ solution in the cell 30 times with an injection interval of 450 s. The "one-set-of-sites" binding model in Microcal Origin 7.0 software was used for data analysis.

Transmission Electron Microscopy (TEM). A drop of each sample in toluene was placed on a carbon-coated copper grid and allowed to evaporate under ambient conditions. A drop of uranyl acetate solution (2 wt %) was placed on the surface of the sample-loaded grid for staining. The sample was deposited for at least 1 min, and excess solution was wicked off by filter paper. The specimen was observed using a JEOL_JEM_3011 HR operating at 300 kV and a JEM-1400 operating at 120 kV. Data were analyzed using Gatan Digital Micrograph software.

Synthesis. $\mathbf{P_{Zn}P_{FB}}$ was prepared by previously reported procedures.[16] The synthesis of $\mathbf{PyP_M}$ is outlined in Scheme 2.

DOI: 10.1021/jacs.5b08092
J. Am. Chem. Soc. 2015, 137, 12394–12399

$P_{Zn}P_{Cu}$. $\mathbf{P_{Zn}P_{FB}}$ (17 mg, 0.0023 mmol) was dissolved in CH_2Cl_2 (100 mL). A methanol (10 mL) solution of copper(II) acetate monohydrate (4.7 mg, 0.024 mmol) was then added to the $\mathbf{P_{Zn}P_{FB}}$ solution. The reaction mixture was stirred at 25 °C for 2 h. The mixture was evaporated for dryness and purified over column chromatography on silica gel using CH_2Cl_2 as an eluent. A freeze-drying procedure using benzene was then performed to give $\mathbf{P_{Zn}P_{Cu}}$ as pink powder. MALDI-TOF-MS *m*/*z*: calcd for $C_{468}H_{508}CuN_{36}O_{24}Zn_8$, 7613.32 [$M^+$ + Na]; found, 7614.858.

1. 4-hydroxybenzaldehyde (6 g, 49.54 mmol), $NaIO_4$ (21.19 g, 99.09 mmol), and NaCl (11.58 g, 198.15 mmol) were dissolved in AcOH/H_2O (9:1) solution (150 mL). KI (16.45g, 99 mmol) was slowly added to the mixture solution over 1 h at 25 °C. Then, the mixture solution was stirred for 2 day at 25 °C. The reaction mixture was poured into distilled water and extracted using EtOAc. The extract was further washed with aqueous $NaHCO_3$. The combined extract was dried over anhydrous $NaSO_4$ and passed through Celite. The solution was evaporated to dryness and then purified by recrystallization using EtOAc and *n*-hexane to give **1** as yellowish powder (10.85 g, 59%). ^{1}H NMR (400 MHz, $CDCl_3$, 25 °C) δ = 9.744 (s, 1 H), 8.203 (s, 2 H), 6.256 (s, 1 H).

2. Under N_2 atmosphere, **1** (10.01 g, 26.77 mmol), K_2CO_3 (5.55 g, 40.16 mmol) were dissolved in *N*,*N*-dimethylformamide (DMF; 95 mL). CH_3I (3.3 mL, 53.54 mmol) was added to the mixture solution and stirred for 13 h at 25 °C. The reaction mixture was poured into distilled water (800 mL). The solid precipitation was collected and washed with distilled water. The residue was dissolved in CH_2Cl_2 and dried over anhydrous $NaSO_4$ and evaporated to dryness to give **2** as yellowish powder (10.15 g, 98%). ^{1}H NMR (400 MHz, $CDCl_3$, 25 °C) δ = 9.812 (s, 1 H), 8.269 (s, 2 H), 3.929 (s, 3 H).

3. $Pd(PPh_3)_2Cl_2$ (7.8 mg, 0.01 mmol), CuI (2.1 mg, 0.01 mmol), and **2** (0.87 g, 2.24 mmol) were dissolved in diisopropylamine (3 mL) and stirred for 1 h at 25 °C under N_2 atmosphere. Trimethylsilylacetylene (0.8 mL, 5.6 mmol) was added to the mixture solution and stirred for 48 h at 25 °C. The reaction mixture was poured into distilled water and extracted with CH_2Cl_2. The extract was dried over anhydrous $NaSO_4$ and then chromatographed on silica gel using CH_2Cl_2 and *n*-hexane as eluents to give **3** (460 mg, 86%). ^{1}H NMR (400 MHz, $CDCl_3$, 25 °C) δ = 9.841 (s, 1 H), 7.84 (s, 2 H), 4.181 (s, 3 H), 0.265 (t, 18 H).

4. In propionic acid (15 mL), **3** (0.64 g, 1.93 mmol) was dissolved. Freshly distilled pyrrole (0.13 mL, 1.93 mmol) was added to the reaction mixture and refluxed for 4 h. The reaction mixture was poured into distilled water and extracted with CH_2Cl_2. The combined extract was dried over anhydrous $NaSO_4$ and then evaporated to dryness. The residue was chromatographed on silica gel using CH_2Cl_2 as an eluent to give crude porphyrin product. The purified porphyrin was dissolved in toluene (30 mL) and excess of nickel(II) acetylacetonate was added. The mixture was refluxed for overnight and then poured into distilled water. The mixture solution was extracted with CH_2Cl_2 and washed with water. The combined extract was dried over anhydrous $NaSO_4$ and then chromatographed on silica gel using CH_2Cl_2 as an eluent to give **4** as dark red solid (410 mg, 55%). ^{1}H NMR (400 MHz, $CDCl_3$, 25 °C) δ = 8.744 (s, 8 H), 8.017 (s, 8 H), 4.316 (s, 12 H), 0.26 (s, 72 H); MALDI-TOF-MS *m*/*z*: calcd for $C_{88}H_{100}N_4NiO_4Si_8$, 1558.53 [$M^+$]; found, 1560.283.

5. To a THF (30 mL) solution of **4** (410 mg, 0.26 mmol), tetrabutylammonium fluoride (13 mL; 10% THF solution) was slowly added at 0 °C, and the reaction mixture was stirred for 24 h at 25 °C. The reaction mixture was poured into distilled water and then extracted with CH_2Cl_2. The combined extract was dried over anhydrous Na_2SO_4 and then purified over column chromatography on silica gel using CH_2Cl_2 as an eluent to give **5** as red solid (110 mg, 43%). ^{1}H NMR (400 MHz, $CDCl_3$, 25 °C) δ = 8.772 (s, 8 H), 8.096 (s, 8 H), 4.356 (s, 12 H), 3.369 (s, 8 H); MALDI-TOF-MS *m*/*z*: calcd for $C_{64}H_{36}N_4NiO_4$, 982.2 [M^+]; found, 982.638.

6. $Pd(PPh_3)_2Cl_2$ (0.89 mg, 0.001 mmol), and 3-iodopyridine (1.02 g, 5 mmol), and **5** (250 mg, 0.25 mmol) were dissolved in diisopropyl amine/THF (2:1) mixture (30 mL). The mixture solution was stirred for 30 min at 60 °C. CuI (0.2 mg, 0.001 mmol) was then added to the mixture solution and further stirred for 2 days at 70 °C. Then the reaction mixture was poured into distilled water and extracted with CH_2Cl_2. The combined extract was evaporated to dryness and purified over recrystallization from CH_2Cl_2/*n*-hexane to give **6** as red solid (330 mg, 82%). MALDI-TOF-MS *m*/*z*: calcd for $C_{104}H_{60}N_{12}NiO_4$, 1599.42 [M^+]; found, 1599.214.

PyP_{FB}. To a CH_2Cl_2 (50 mL) solution of **6** (330 mg, 0.21 mmol), sulfuric acid (1 mL), methanol (10 mL), and THF (10 mL) were added and stirred for 30 min at 25 °C. The reaction mixture was poured into aqueous $NaHCO_3$ and extracted with CH_2Cl_2. The combined extract was purified over recrystallization from CH_2Cl_2/*n*-hexane to give $\mathbf{PyP_{FB}}$. ^{1}H NMR (400 MHz, $CDCl_3$, 25 °C) δ = 9.016 (s, 8 H), 8.839−8.836 (m, 8 H), 8.819−8.816 (m, 8 H), 8.580 (m, 8 H), 8.572−8.569 (m, 8 H), 8.396 (s, 8 H), 4.500 (s, 12 H), −2.813 (s, 2 H); ^{13}C NMR (400 MHz, $CDCl_3$, 25 °C) δ = 162.08, 152.51, 149.24, 143.41, 139.68, 138.82, 137.64, 123.36, 120.36, 118.25, 115.68, 91.19, 88.48, 62.18; MALDI-TOF-MS *m*/*z*: calcd for $C_{104}H_{62}N_{12}O_4$, 1543.51 [M^+]; found, 1542.703.

PyP_{Cu}. To a CH_2Cl_2 (100 mL) solution of $\mathbf{PyP_{FB}}$ (10.8 mg, 0.007 mmol), $Cu(OAc)_2{\cdot}H_2O$ (3.1 mg, 0.02 mmol), and methanol (3 mL) were added and stirred for 3 h at 25 °C. The reaction mixture solution was poured into water and extracted with CH_2Cl_2. The combined extract was purified over column chromatography on silica gel using CH_2Cl_2 as the eluent to give $\mathbf{PyP_{Cu}}$. MALDI-TOF-MS *m*/*z*: calcd for $C_{104}H_{60}CuN_{12}O_4$, 1604.42 [M^+]; found, 1604.273.

RESULTS AND DISCUSSION

Multiporphyrin dendrimers and multipyridyl dendrimers were synthesized for the formation of supramolecular coordination polymers. The synthesis of $\mathbf{P_{Zn}P_{FB}}$ was carried out by previously reported procedures.[16] Cupper ion was inserted to $\mathbf{P_{Zn}P_{FB}}$ using $Cu(OAc)_2{\cdot}H_2O$ to get $\mathbf{P_{Zn}P_{Cu}}$. The synthesis of $\mathbf{PyP_M}$ is outlined in Scheme 2. First, 3,5-diiodo-4-hydroxy benzaldehyde (**1**) was prepared from 4-hydroxy benzaldehyde. Then, the hydroxyl group of **1** was methylated using CH_3I to get **2**. Trimethylsilylacetylene (TMS-acetylene) groups were introduced to **2** through Sonogashira's coupling reaction to obtain **3**.[36] Acid-catalyzed annulation reaction of **3** with pyrrole and successive oxidation was performed to obtain porphyrin. To prevent copper insertion in next step, nickel(II) acetylacetonate was reacted to get TMS-acetylene bearing nickel porphyrin (**4**). After the deprotection of TMS group, 3-iodopyridine was introduced through Sonogashira's coupling reaction to get **6**. Finally, $\mathbf{PyP_{FB}}$ and $\mathbf{PyP_{Cu}}$ were prepared by demetalation and successive copper coordination. The porphyrins were characterized by NMR and MALDI-TOF-MS analysis.

The pyridyl groups in $\mathbf{PyP_M}$ can be bound to the $\mathbf{P_{Zn}}$s in $\mathbf{P_{Zn}P_M}$ as axial ligands for the formation of supramolecular assemblies.[37−40] Because $\mathbf{P_{Zn}P_M}$ and $\mathbf{PyP_M}$ have eight $\mathbf{P_{Zn}}$s and pyridyl groups, respectively, the stoichiometry for saturation binding would be 1:1. UV−vis spectral changes upon titration of $\mathbf{PyP_{FB}}$ to $\mathbf{P_{Zn}P_{FB}}$ were measured in toluene at 25 °C to investigate the dynamics of supramolecular assembly formation. Because the absorption bands of $\mathbf{PyP_{FB}}$ and $\mathbf{P_{Zn}P_{FB}}$ overlapped widely (Figure S1a), differential spectra were recorded by subtracting the absorption spectra of both pure $\mathbf{PyP_{FB}}$ and $\mathbf{P_{Zn}P_{FB}}$ from that of mixture solutions. As shown in Figure 1a, the differential spectra exhibited clear isosbestic points at 414.5, 543.5, and 574.0 nm upon successive addition of $\mathbf{PyP_{FB}}$, indicating binding of pyridyl groups to $\mathbf{P_{Zn}}$s to generate a new type of self-assembled species. As expected, the maximum spectral changes were observable at 1 equiv addition of $\mathbf{PyP_{FB}}$. The binding isotherm reached a maximum value at 1 equiv addition, and then the value decreased gradually (Figure 1b).

DOI: 10.1021/jacs.5b08092
J. Am. Chem. Soc. 2015, 137, 12394−12399

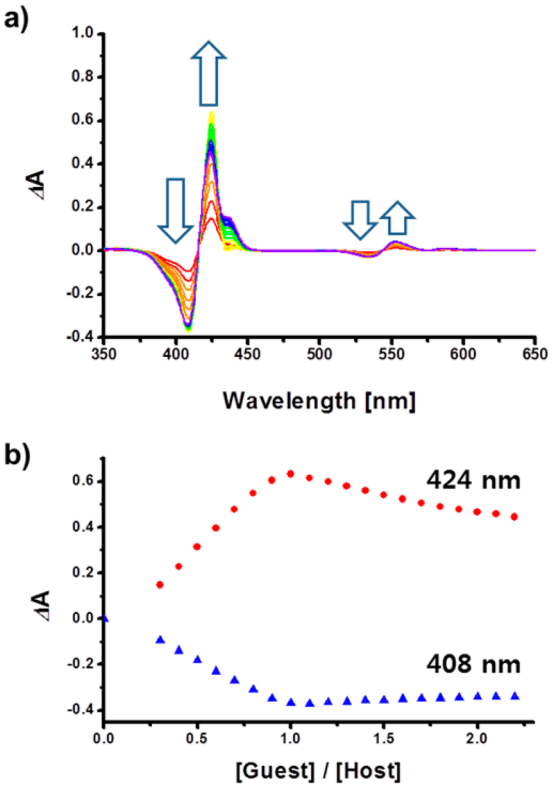

Figure 1. (a) Differential absorption spectra upon titration of $\mathbf{PyP}_{FB}$ (0–2.2 equiv) to $\mathbf{P}_{Zn}\mathbf{P}_{FB}$ in toluene at 25 °C and (b) binding isotherms of the UV–vis titration monitored at 424 and 408 nm.

Job's plot analysis (Figure S1b) also indicated 1:1 stoichiometry of saturation binding.[41] Based on the molecular shapes and absorption changes, we expected that $\mathbf{PyP}_M$ and $\mathbf{P}_{Zn}\mathbf{P}_M$ would form fibrous coordination polymers at 1:1 stoichiometry as illustrated in Scheme 1. The eight $\mathbf{P}_{Zn}$ wings linked to the meso-phenyl groups of $\mathbf{P}_{Zn}\mathbf{P}_M$, which are conformationally orthogonal to the plane of $\mathbf{P}_{FB}$ or $\mathbf{P}_{cu}$. Therefore, four $\mathbf{P}_{Zn}$s are located onto the half side of $\mathbf{P}_{Zn}\mathbf{P}_M$. In the same respect, eight pyridyl groups are linked to the meso-phenyl groups of core porphyrins in $\mathbf{PyP}_M$. Considering the three-dimensional structures of $\mathbf{P}_{Zn}\mathbf{P}_M$ and $\mathbf{PyP}_M$, only four pyridyl groups in a $\mathbf{PyP}_M$ can simultaneously interact with the $\mathbf{P}_{Zn}$s in a $\mathbf{P}_{Zn}\mathbf{P}_M$. When $\mathbf{P}_{Zn}\mathbf{P}_M$ and $\mathbf{PyP}_M$ form 1:1 coordination complex, four pyridyl groups and $\mathbf{P}_{Zn}$s still remained in the opposite side, and thus it forces the multiple axial coordination interactions of pyridyl groups to $\mathbf{P}_{Zn}$s continuously, resulting in the fibrous supramoelcular coordination polymer. If an excess amount of $\mathbf{PyP}_M$ was added to $\mathbf{P}_{Zn}\mathbf{P}_M$, the fibrous assembly may be shortened by insertion of $\mathbf{PyP}_M$ into polymer chain, which might become the terminal of the supramolecular polymers. If the amount of $\mathbf{PyP}_M$ addition exceeds 2 equiv, $\mathbf{P}_{Zn}\mathbf{P}_M$ and $\mathbf{PyP}_M$ may form a sandwich-type 1:2 assembly.

Thermodynamics of the self-assembly process were investigated by ITC. The isothermal titration curve exhibited strong exothermic peaks for each injection of $\mathbf{PyP}_{FB}$ to $\mathbf{P}_{Zn}\mathbf{P}_{FB}$ (Figure 2). Exothermic peaks gradually decreased and finally disappeared by successive addition of $\mathbf{PyP}_{FB}$. Because the titration curve matched that for typical 1:1 binding host–guest systems, we used a simple 1:1 binding model to estimate thermodynamic parameters.[42−44] Curve fitting revealed apparent $\Delta H°$, $\Delta G°$, $\Delta S°$, and association constant (K_{ass}) values of -5.82×10^4 J/mol, -1.00×10^4 J/mol, -166 J/mol K, and 2.91×10^6 M^{-1}, respectively. The association constant was high enough for a fibrous assembly to form at micromolar concentrations.

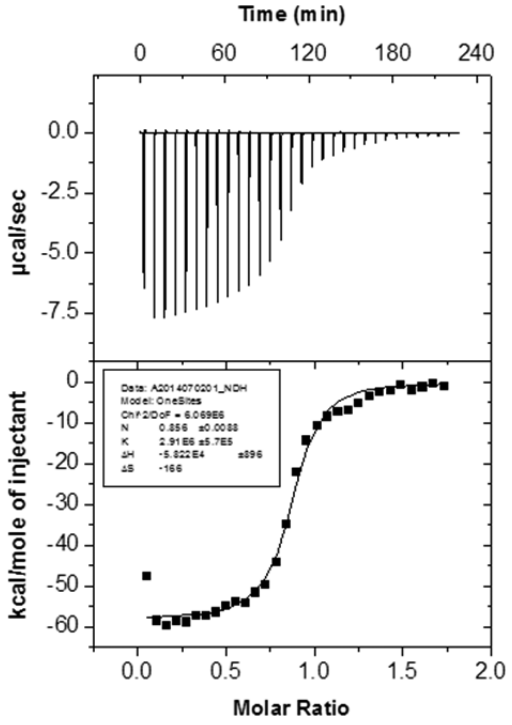

Figure 2. Result of ITC upon titration of $\mathbf{PyP}_{FB}$ to $\mathbf{P}_{Zn}\mathbf{P}_{FB}$ in toluene at 25 °C.

^{1}H NMR study was conducted to confirm supramolecular coordination polymer formation. As shown in Figure 3, both

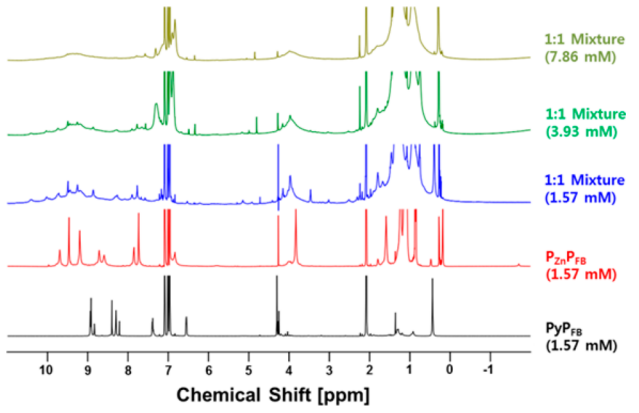

Figure 3. ^{1}H NMR spectra (600 MHz, toluene-d_8, 25 °C) of $\mathbf{P}_{Zn}\mathbf{P}_{FB}$, $\mathbf{PyP}_{FB}$, and supramolecular polymer formed from 1:1 ratio of $\mathbf{P}_{Zn}\mathbf{P}_{FB}$ and $\mathbf{PyP}_{FB}$ with different concentrations (1.57, 3.93, and 7.86 mM).

$\mathbf{P}_{Zn}\mathbf{P}_{FB}$ and $\mathbf{PyP}_{FB}$ exhibits relatively sharp ^{1}H signals, whereas 1:1 mixtures of $\mathbf{P}_{Zn}\mathbf{P}_{FB}$ and $\mathbf{PyP}_{FB}$ exhibit significant broadening of signals, indicating that the conformational fluctuations become slower than the NMR time scale due to formation of large supramolecular polymers. Moreover, the degree of broadening increases by increasing concentration of 1:1 mixture. Diffusion coefficients (D) of $\mathbf{P}_{Zn}\mathbf{P}_{FB}$, $\mathbf{PyP}_{FB}$, and 1:1 mixture of $\mathbf{P}_{Zn}\mathbf{P}_{FB}$ and $\mathbf{PyP}_{FB}$ were measured by 2D DOSY NMR spectroscopy (Figure S2). As a result, D value of $\mathbf{P}_{Zn}\mathbf{P}_{FB}$ and $\mathbf{PyP}_{FB}$ showed 1.06×10^{-8} m^2 s^{-1} and 1.11×10^{-8} $m^2 s^{-1}$, whereas 1:1 mixture of $\mathbf{P}_{Zn}\mathbf{P}_{FB}$ and $\mathbf{PyP}_{FB}$ exhibited relatively lower D value of 7.19×10^{-9} m^2 s^{-1} than those of $\mathbf{P}_{Zn}\mathbf{P}_{FB}$ and

DOI: 10.1021/jacs.5b08092
J. Am. Chem. Soc. 2015, 137, 12394–12399

PyP_{FB} at the same concentration (1.57 mM). When concentration was increased to 7.86 mM, the D value of 1:1 mixture was greatly decreased to 2.62×10^{-9} m^2 s^{-1} with broad distribution, indicating concentration-dependent molecular size increasing of supramolecular coordination polymer.

The formation of a fibrous assembly from $P_{Zn}P_{FB}$ and PyP_{FB} was visualized by AFM and TEM. For AFM observation, a 1:1 mixture solution of $P_{Zn}P_{FB}$ and PyP_{FB} (20 μM) in toluene was cast onto mica. As shown in Figure 4a, fibrous assemblies with

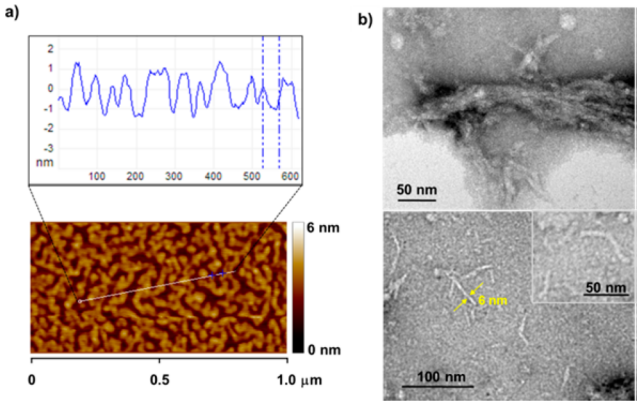

Figure 4. Microscopic observations of supramolecular polymer: (a) AFM and (b) TEM images.

regular height (ca. 2 nm) were observed. The 1:1 mixture solution of $P_{Zn}P_{FB}$ and PyP_{FB} (0.1 wt %) was stained with 2 wt % uranyl acetate for TEM observation. Considering the expected thickness of assembled fibers consisting of rigid porphyrin parts and fully extended geometry of peripheral alkyl chains, the measured thickness about 2 nm in the AFM image seems to be attributed to the flattening of nanofibers due to the substrate effect. However, additional TEM observation of 1:1 mixture solution of $P_{Zn}P_{FB}$ and PyP_{FB} (0.1 wt %) clearly showed the formation of nanofibers with a regular diameter of ca. 6 nm (Figure 4b), which is reasonable as compared to the cross-sectional dimension of 1D fibrils.

In our previous reports, we have demonstrated the efficient energy transfer from P_{Zn}s to the focal P_{FB} in $P_{Zn}P_{FB}$. Upon excitation at 414 nm, $P_{Zn}P_{FB}$ exhibited intense emission bands around 650 and 720 nm, originating from the focal P_{FB} with a very weak shoulder around 600 nm from the P_{Zn} wings (Figure 5a), where the energy-transfer efficiency was estimated to be 94%.[30] The efficient energy-transfer dynamics in $P_{Zn}P_{FB}$ can be changed by the formation of supramolecular assembly with PyP_{FB}. Figure 5b shows fluorescence emission changes of $P_{Zn}P_{FB}$ in response to the addition of PyP_{FB} upon excitation at 414 nm. According to the addition of PyP_{FB}, the emission band around 600 nm, originated from P_{Zn} wings, completely vanished, and the emission bands around 650 and 720 nm from P_{FB} were slightly red-shifted. Notably, the emission maximum wavelengths were coincident with those from PyP_{FB}. This observation suggests that the excitation energy of P_{Zn} wings flows to the PyP_{FB} due to formation of a fibrous assembly. In other words, intramolecular energy transfer from P_{Zn} wings to the focal P_{FB} in $P_{Zn}P_{FB}$ changes to intermolecular energy transfer to the PyP_{FB}. The change in energy transfer was more distinctly observable when nonfluorescent copper porphyrins (P_{Cu}) were used.[45] For this experiment, we newly prepared nonfluorescent $P_{Zn}P_{Cu}$ and PyP_{Cu}. As shown in Figure 5a, $P_{Zn}P_{Cu}$ exhibits very weak fluorescence emission

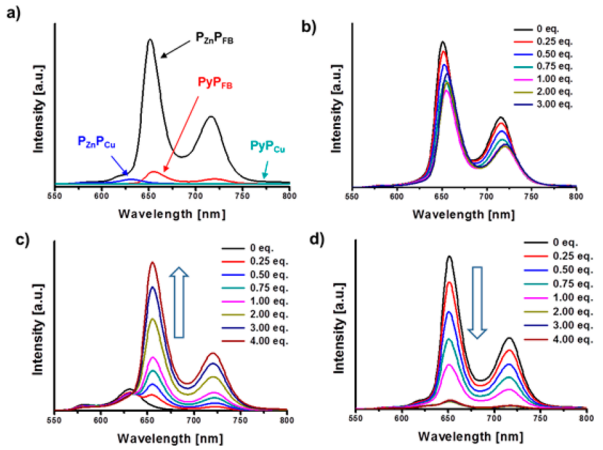

Figure 5. Emission changes by supramolecular assembly formations. (a) Emission spectra of $P_{Zn}P_{FB}$, $P_{Zn}P_{Cu}$, PyP_{FB}, and PyP_{Cu}; (b) emission changes of $P_{Zn}P_{FB}$ by successive addition of PyP_{Cu}; (c) emission changes of $P_{Zn}P_{Cu}$ by successive addition of PyP_{FB}; (d) emission changes of $P_{Zn}P_{FB}$ by successive addition of PyP_{Cu}. All emission spectra were measured in toluene at 25 °C.

from P_{Zn}s around 580 and 630 nm due to efficient energy transfer from P_{Zn}s to the nonfluorescent focal P_{Cu}. When PyP_{FB} was added to $P_{Zn}P_{Cu}$, strong emission peaks were generated at 655 and 724 nm, coincident with the emission bands of PyP_{FB} (Figure 5c). In contrast, the weak emission from P_{Zn} wings, around 570 and 630 nm, was further decreased. Due to formation of coordination polymers, the excitation energy of P_{Zn} wings in $P_{Zn}P_{Cu}$ flows to PyP_{FB} instead of the focal P_{Cu} in dendrimer. However, we cannot absolutely exclude the direct excitation of PyP_{FB} in this experiment. Therefore, nonfluorescent PyP_{Cu} was titrated to fluorescent $P_{Zn}P_{FB}$. The strong emission of $P_{Zn}P_{FB}$ decreased gradually in response to the addition of PyP_{Cu} (Figure 5d). Notably, the decrease in fluorescence intensity of PyP_{FB} was stopped after a 2 equiv addition of PyP_{Cu}, indicating excess PyP_M addition makes 1:2 complexes. The results of fluorescence titration experiments consistent with our assumption that intramolecular energy transduction changes to intermolecular energy transduction by the formation of supramolecular coordination polymers.

CONCLUSIONS

Fibrous supramolecular coordination polymers were formed from artificial light-harvesting multiporphyrin dendrimers and multipyridyl porphyrins through axial coordination interactions of pyridyl groups to P_{Zn}. Formation of coordination polymers greatly reduced intramolecular energy transfer within the artificial light-harvesting dendrimer, and a new pathway of intermolecular energy transfer became predominant. Such a molecularly modulated energy-transfer phenomena can be used as a motif in the design of new photofunctional materials.

ASSOCIATED CONTENT

Supporting Information

The Supporting Information is available free of charge on the ACS Publications website at DOI: 10.1021/jacs.5b08092.

Additional spectral data (Figures S1–2) (PDF)

AUTHOR INFORMATION

Corresponding Authors

*wdjang@yonsei.ac.kr

DOI: 10.1021/jacs.5b08092
J. Am. Chem. Soc. 2015, 137, 12394–12399

*eunjilee@cnu.ac.kr

Notes

The authors declare no competing financial interest.

■ ACKNOWLEDGMENTS

This work was supported by the Mid-Career Researcher Program (2014R1A2A1A10051083) and the Basic Science Research Program (2013R1A1A2061197) funded by the National Research Foundation (NRF) of Korea.

■ REFERENCES

(1) Aida, T.; Meijer, E.; Stupp, S. *Science* **2012**, *335*, 813.
(2) Yang, L.; Tan, X.; Wang, Z.; Zhang, X. *Chem. Rev.* **2015**, *115*, 7196.
(3) Ma, X.; Tian, H. *Acc. Chem. Res.* **2014**, *47*, 1971.
(4) Dong, S.; Zheng, B.; Wang, F.; Huang, F. *Acc. Chem. Res.* **2014**, *47*, 1982.
(5) de Greef, T. F.; Meijer, E. *Nature* **2008**, *453*, 171.
(6) Saeki, A.; Koizumi, Y.; Aida, T.; Seki, S. *Acc. Chem. Res.* **2012**, *45*, 1193.
(7) Yan, X.; Cook, T. R.; Pollock, J. B.; Wei, P.; Zhang, Y.; Yu, Y.; Huang, F.; Stang, P. J. *J. Am. Chem. Soc.* **2014**, *136*, 4460.
(8) Liu, Y.; Huang, Z.; Tan, X.; Wang, Z.; Zhang, X. *Chem. Commun.* **2013**, *49*, 5766.
(9) Wei, P.; Yan, X.; Huang, F. *Chem. Soc. Rev.* **2015**, *44*, 815.
(10) Albrecht, M. *Nat. Chem.* **2014**, *6*, 761.
(11) Li, W.; Kim, Y.; Li, J.; Lee, M. *Soft Matter* **2014**, *10*, 5231.
(12) Satake, A.; Kobuke, Y. *Tetrahedron* **2005**, *61*, 13.
(13) Choi, M. S.; Aida, T.; Yamazaki, T.; Yamazaki, I. *Angew. Chem.* **2001**, *113*, 3294.
(14) Choi, M. S.; Aida, T.; Yamazaki, T.; Yamazaki, I. *Chem. - Eur. J.* **2002**, *8*, 2667.
(15) Imahori, H. *J. Phys. Chem. B* **2004**, *108*, 6130.
(16) Jang, W.-D.; Lee, C.-H.; Choi, M.-S.; Osada, M. *J. Porphyrins Phthalocyanines* **2009**, *13*, 787.
(17) Uetomo, A.; Kozaki, M.; Suzuki, S.; Yamanaka, K.-i.; Ito, O.; Okada, K. *J. Am. Chem. Soc.* **2011**, *133*, 13276.
(18) Hajjaj, F.; Yoon, Z. S.; Yoon, M.-C.; Park, J.; Satake, A.; Kim, D.; Kobuke, Y. *J. Am. Chem. Soc.* **2006**, *128*, 4612.
(19) Wasielewski, M. R. *Acc. Chem. Res.* **2009**, *42*, 1910.
(20) Hu, X.; Damjanović, A.; Ritz, T.; Schulten, K. *Proc. Natl. Acad. Sci. U. S. A.* **1998**, *95*, 5935.
(21) Scholes, G. D.; Fleming, G. R.; Olaya-Castro, A.; van Grondelle, R. *Nat. Chem.* **2011**, *3*, 763.
(22) Aratani, N.; Kim, D.; Osuka, A. *Acc. Chem. Res.* **2009**, *42*, 1922.
(23) Brodard, P.; Matzinger, S.; Vauthey, E.; Mongin, O.; Papamicaël, C.; Gossauer, A. *J. Phys. Chem. A* **1999**, *103*, 5858.
(24) Choi, M. S.; Yamazaki, T.; Yamazaki, I.; Aida, T. *Angew. Chem., Int. Ed.* **2004**, *43*, 150.
(25) Hori, T.; Aratani, N.; Takagi, A.; Matsumoto, T.; Kawai, T.; Yoon, M. C.; Yoon, Z. S.; Cho, S.; Kim, D.; Osuka, A. *Chem. - Eur. J.* **2006**, *12*, 1319.
(26) Yang, J.; Yoon, M.-C.; Yoo, H.; Kim, P.; Kim, D. *Chem. Soc. Rev.* **2012**, *41*, 4808.
(27) Kim, D.; Heo, J.; Ham, S.; Yoo, H.; Lee, C.-H.; Yoon, H.; Ryu, D.; Kim, D.; Jang, W.-D. *Chem. Commun.* **2011**, *47*, 2405.
(28) Neuhaus, P.; Cnossen, A.; Gong, J. Q.; Herz, L. M.; Anderson, H. L. *Angew. Chem., Int. Ed.* **2015**, *54*, 7344.
(29) Kondratuk, D. V.; Perdigão, L. M.; Esmail, A. M.; O'Shea, J. N.; Beton, P. H.; Anderson, H. L. *Nat. Chem.* **2015**, *7*, 317.
(30) Jeong, Y. H.; Son, M.; Yoon, H.; Kim, P.; Lee, D. H.; Kim, D.; Jang, W. D. *Angew. Chem.* **2014**, *126*, 7045.
(31) Krishna Kumar, R.; Balasubramanian, S.; Goldberg, I. *Inorg. Chem.* **1998**, *37*, 541.
(32) Parkinson, P.; Knappke, C. E.; Kamonsutthipaijit, N.; Sirithip, K.; Matichak, J. D.; Anderson, H. L.; Herz, L. M. *J. Am. Chem. Soc.* **2014**, *136*, 8217.
(33) Son, H.-J.; Jin, S.; Patwardhan, S.; Wezenberg, S. J.; Jeong, N. C.; So, M.; Wilmer, C. E.; Sarjeant, A. A.; Schatz, G. C.; Snurr, R. Q.; Farha, O. K.; Wiederrecht, G. P.; Hupp, J. T. *J. Am. Chem. Soc.* **2013**, *135*, 862.
(34) Yoon, H.; Lee, C. H.; Jang, W. D. *Chem. - Eur. J.* **2012**, *18*, 12479.
(35) Yoon, H.; Lim, J. M.; Gee, H.-C.; Lee, C.-H.; Jeong, Y.-H.; Kim, D.; Jang, W.-D. *J. Am. Chem. Soc.* **2014**, *136*, 1672.
(36) Sonogashira, K.; Tohda, Y.; Hagihara, N. *Tetrahedron Lett.* **1975**, *16*, 4467.
(37) Zhang, Z.; Hu, R.; Liu, Z. *Langmuir* **2000**, *16*, 1158.
(38) Chambron, J. C.; Harriman, A.; Heitz, V.; Sauvage, J. P. *J. Am. Chem. Soc.* **1993**, *115*, 6109.
(39) Kobuke, Y.; Miyaji, H. *J. Am. Chem. Soc.* **1994**, *116*, 4111.
(40) Williams, D. E.; Rietman, J. A.; Maier, J. M.; Tan, R.; Greytak, A. B.; Smith, M. D.; Krause, J. A.; Shustova, N. B. *J. Am. Chem. Soc.* **2014**, *136*, 11886.
(41) Connors, K. A. *Binding constants: the measurement of molecular complex stability*; Wiley-Interscience: Hoboken, NJ, 1987.
(42) Lee, H. H.; Choi, T. S.; Lee, S. J. C.; Lee, J. W.; Park, J.; Ko, Y. H.; Kim, W. J.; Kim, K.; Kim, H. I. *Angew. Chem.* **2014**, *126*, 7591.
(43) Lin, F.; Zhan, T.-G.; Zhou, T.-Y.; Zhang, K.-D.; Li, G.-Y.; Wu, J.; Zhao, X. *Chem. Commun.* **2014**, *50*, 7982.
(44) Song, N.; Chen, D.-X.; Qiu, Y.-C.; Yang, X.-Y.; Xu, B.; Tian, W.; Yang, Y.-W. *Chem. Commun.* **2014**, *50*, 8231.
(45) Schick, G. A.; Schreiman, I. C.; Wagner, R. W.; Lindsey, J. S.; Bocian, D. F. *J. Am. Chem. Soc.* **1989**, *111*, 1344.

DOI: 10.1021/jacs.5b08092
J. Am. Chem. Soc. 2015, 137, 12394−12399